

Nanomechanical and structural characteristics of nanodiamond composite films dependent on target-substrate distance.

EGIZA, M., DIAB, M.R., MURASAWA, K., NARAGINO, H. and YOSHITAKE, T.

2025

© The Author(s) 2024.



Nanomechanical and Structural Characteristics of Nanodiamond Composite Films Dependent on Target-Substrate Distance

Mohamed Egiza^{1,2} · Mohamed Ragab Diab^{1,3} · Koki Murasawa^{3,4} · Hiroshi Naragino³ · Tsuyoshi Yoshitake³

Received: 15 December 2023 / Accepted: 6 May 2024 / Published online: 18 June 2024
© The Author(s) 2024

Abstract

This study explores the optimization of target-substrate distance (TSD) in coaxial arc plasma deposition technique for depositing nanodiamond composite (NDC) films on unheated WC–Co substrates, with a focus on enhancing properties relevant to cutting tool applications. TSD significantly impacted film growth and adhesion, while hardness and Young's modulus remained stable within the 10–50 mm TSD range. Increased TSD led to reduced deposition rates and film thickness, but improved quality by eliminating macroparticles and reducing surface roughness. Notably, the NDC film deposited at 10 mm TSD exhibited exceptional adhesion resistance, a thickness of 11.45 μm , low compressive internal stress (2.8 GPa), and a surface roughness (S_a) of 280 nm, coupled with an impressive hardness of 49.12 GPa. This film also achieved a favorable deposition rate of 1.05 nm/s. In comparison, the film deposited at 15 mm TSD displayed a maximum hardness of 51.3 GPa, lower S_a of 179 nm, but a reduced deposition rate of 0.29 nm/s. The estimated C_{sp^3} fraction correlated well with the nanoindentation measurements, while internal stress showed a consistent relationship with film adhesion. These findings suggest that a TSD of 10 mm is optimal for balancing hardness, adhesion, deposition rate, and surface roughness, making NDC films a promising candidate for cutting tool applications.

Keywords Hard coatings · DLC · Coaxial arc plasma · Target-substrate distance · Internal stress · XPS

1 Introduction

The application of protective hard films on WC–Co cutting tools, including inserts, drill bits, and end mills, is a common practice to enhance tool lifespan and improve cutting quality, especially for challenging materials like carbon fiber-reinforced polymers (CFRP), Si–Al alloys, and SiC [1, 2]. Despite the apparent fracture toughness of WC–Co alloys,

their hardness degrades during manufacturing due to the presence of Co as a bonding phase [3–5]. This degradation leads to wear resistance reduction, making protective coatings with high hardness crucial. Diamond, with exceptional hardness, emerges as a promising candidate among various hard coatings [6–9]. Additionally, low surface roughness is vital for consistent cutting quality and improved sliding properties, a characteristic efficiently achieved by cost-effective diamond-like carbon (DLC) films [10].

Diamond films have been grown using chemical vapor deposition (CVD) techniques, such as hot filament CVD [7, 9, 11] and microwave plasma-assisted CVD [12, 13]. Conversely, DLC films can be deposited through various physical vapor deposition (PVD) and CVD methods [14–18], including ion plating, magnetron sputtering, plasma-enhanced CVD, and the filtered cathodic vacuum arc process (FCVA). The FCVA can deposit the hardest DLC variant known as tetrahedral amorphous carbon (ta-C) with hardness comparable to diamond [19]. However, the substrate's elevated temperature during diamond growth (700–800 °C) negatively tailors properties of WC–Co substrate and enhances Co's catalytic effects, which degrades film adhesion. Surprisingly,

✉ Mohamed Egiza
m.egiza@rgu.ac.uk

✉ Tsuyoshi Yoshitake
Tsuyoshi_yoshitake@kyudai.jp

¹ Department of Mechanical Engineering, Kafrelsheikh University, Kafrelsheikh 33516, Egypt

² School of Engineering, Robert Gordon University, Garthdee Road, Aberdeen AB10 7GJ, UK

³ Department of Advanced Energy Science and Engineering, Faculty of Engineering Sciences, Kyushu University, Kasuga, Fukuoka 816-8580, Japan

⁴ OSG Corporation, 3-22 Honnogahara, Toyokawa, Aichi 442-8543, Japan



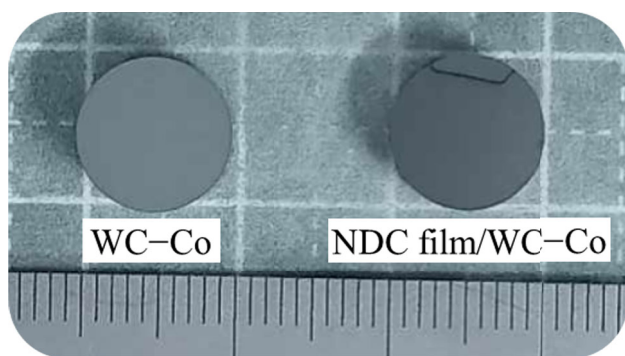


Fig. 1 Typical images of the WC–Co substrate with and without the NDC film

ta–C films can be deposited at lower substrate temperatures or even without external heating, but their limited thickness (less than 1000 nm) and high internal stress (up to 9 GPa) pose challenges.

Coaxial arc plasma deposition (CAPD) presents a promising new approach for depositing hard coatings on WC–Co tools [20–24]. This method allows for the creation of nanodiamond composite (NDC) films. These films combine the exceptional hardness of diamond nanocrystals with the beneficial properties of an amorphous carbon matrix [27]. NDC films boast impressive characteristics, including high hardness (≥ 50 GPa), substantial thickness ($\geq 7 \mu\text{m}$), low internal stress (≤ 4.5 GPa), a high sp^3 fraction (70%), and a significant deposition rate (40 nm/min) [25, 26]. Importantly, CAPD allows for deposition at lower substrate temperatures compared to diamond CVD, minimizing negative impacts on the WC–Co substrate.

The characteristics of NDC films are highly dependent on the specific CAPD conditions employed. Various parameters, such as arc discharge repetition rate, base pressure, substrate temperature, deposition power, target and gas types, and substrate material itself, can influence the films' structural, mechanical, optical, and tribological properties [28, 29]. Optimizing these parameters is crucial for tailoring NDC film properties to achieve superior performance in WC–Co cutting tools.

While several studies have explored the influence of CAPD deposition parameters on NDC characteristics, limited attention has been given to the correlation between some deposition parameters and film qualities. Among the studied parameters, arc discharge repetition rate and substrate temperature significantly influence the mechanical properties of NDC coatings deposited on WC–Co substrates [30]. Lower repetition rates (1 Hz) and the absence of external heating resulted in NDC films with a hardness of 51 GPa, a Young's modulus of 520 GPa, and a thickness of approximately $3 \mu\text{m}$. Conversely, increasing the substrate temperature to 550°C at a 5 Hz repetition rate led to a significant decrease in film

hardness to 17.3 GPa. Similarly, increasing the repetition rate from 1 to 5 Hz without external heating resulted in a decline in hardness to 31.8 GPa [30]. These findings suggest an inverse relationship between hardness and both repetition rate and substrate temperature.

Applying a negative bias voltage to WC–Co substrates during deposition at 40–80 kHz [31] enhanced the deposition rate and film thickness. However, this process also strengthened sp^2 bonds within the film structure, consequently reducing its overall hardness.

Doping studies incorporating metallic (Cr) [24] and non-metallic (Si and B) elements [32–34] demonstrated varying impacts on film hardness. Under optimized conditions, a notable improvement in both hardness and deposition rate was observed. Specifically, the inclusion of 1 at% Si or B dopant led to a remarkable increase in hardness from 51 GPa to 58–60 GPa. This enhancement highlights the potential for achieving thicker films ($7 \mu\text{m}$) with improved deposition efficiency (shorter deposition times).

The type of substrate plays a crucial role in both the applicability and deposition of NDC films. While Si substrates necessitate external heating for successful deposition [21, 35], Ti substrates require pre-treatment with an ion etching gun to remove the oxide layer and ensure good film adhesion [36]. In contrast, WC–Co substrates demonstrate good adhesion without external heating or treatments typically required for diamond growth, such as Co etching and nanodiamond seeding [37, 38]. This eliminates the need for additional and potentially complex pre-deposition steps for WC–Co substrates.

CAPD holds a promise to deposit high-performance NDC films on WC–Co cutting tools. However, a critical knowledge gap exists: the specific impact of target-substrate distance (TSD) on crucial film properties remains largely unexplored. This gap hinders the optimization of CAPD for achieving desired NDC film characteristics. Precise control of TSD is essential in various PVD methods for influencing film properties across diverse materials. Optimal TSD values lead to increased layer thickness and a higher $sp^3/(sp^3 + sp^2)$ ratio in coatings like titanium aluminum nitride [39], SZO [40], and a-C [41]. This translates to improved hardness and superior electrical resistivity. Similarly, for NDC films deposited on WC–Co substrates using CAPD, adjusting TSD is crucial for crafting high-quality films with the desired mechanical attributes.

By investigating the correlation between TSD and key NDC film characteristics, including thickness, deposition rate, surface roughness, internal stress, and the sp^3 fraction (linked to hardness), this research aims to address the critical knowledge gap. Filling this gap is vital to unlocking the full potential of CAPD for creating superior NDC coatings for WC–Co cutting tools. This will lead to extended tool



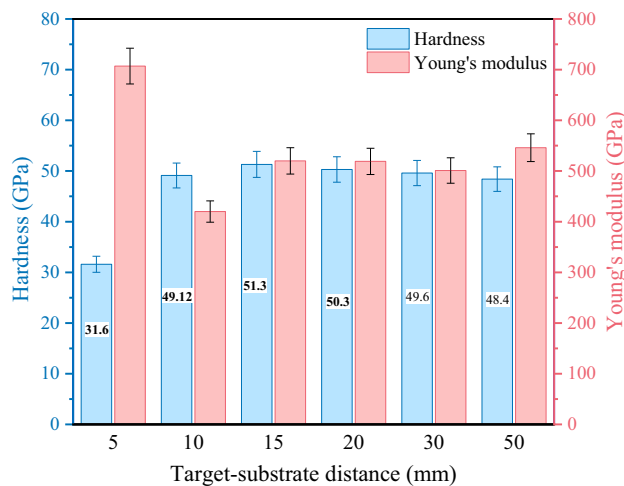


Fig. 2 Nanoindentation measurements assessing NDC film properties at different target-substrate distances (TSDs) in the range of 5–50 mm

lifespan, enhanced cutting performance, and cost-effective production.

In this study, NDC films were deposited on unheated WC–Co substrates at various TSDs (5–50 mm), aiming to identify the optimal TSD for achieving thick films ($> 10 \mu\text{m}$) comparable to diamond, achieving high deposition rates for cost-effectiveness, maintaining low surface roughness similar to DLC films, ensuring lower internal stress for good film adhesion, and attaining a high C sp^3 fraction for enhanced hardness. This research seeks to provide valuable insights into the correlation between target-substrate distance and NDC film characteristics.

2 Experimental Procedures

2.1 Films Synthesis

NDC films were systematically deposited onto WC–Co substrates (K-type cemented carbide, $\varnothing 10 \times 4.5 \text{ mm}$) using coaxial arc plasma deposition (CAPD) technique. The CAPD employed a coaxial arc plasma gun (ULVAC, APG-1000) equipped with a graphite rod (99.99% purity, $\varnothing 10 \times 30 \text{ mm}$), following the configuration detailed in previous references [23, 31, 42]. The orientation of the coaxial arc plasma gun head was directed toward the WC–Co substrates, with varying distances between the end of graphitic target and the substrate surface set at 5, 10, 15, 20, 30, and 50 mm. Preceding the film deposition, the vacuum chamber underwent evacuation by a turbomolecular pump, reaching a base pressure of less than 10^{-4} Pa . The arc plasma gun, operated with a $720 \mu\text{F}$ capacitor, was subjected to a 100 V voltage supply pulsating at a frequency of 1 Hz. The deposition was carried out at base pressure with no gas flow or applying external heat

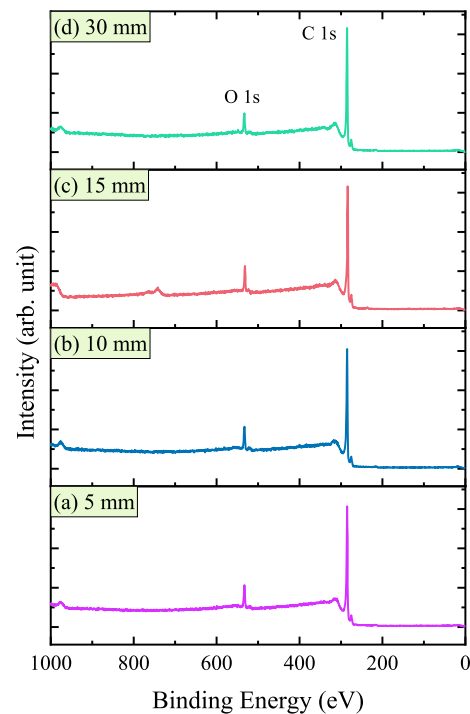


Fig. 3 XPS survey of NDC films at different TSDs: (a) 5, (b) 10, (c) 15, and (d) 30 mm

on the substrates. Figure 1 illustrates a typical image showing the WC–Co substrate along with the NDC film deposited on it.

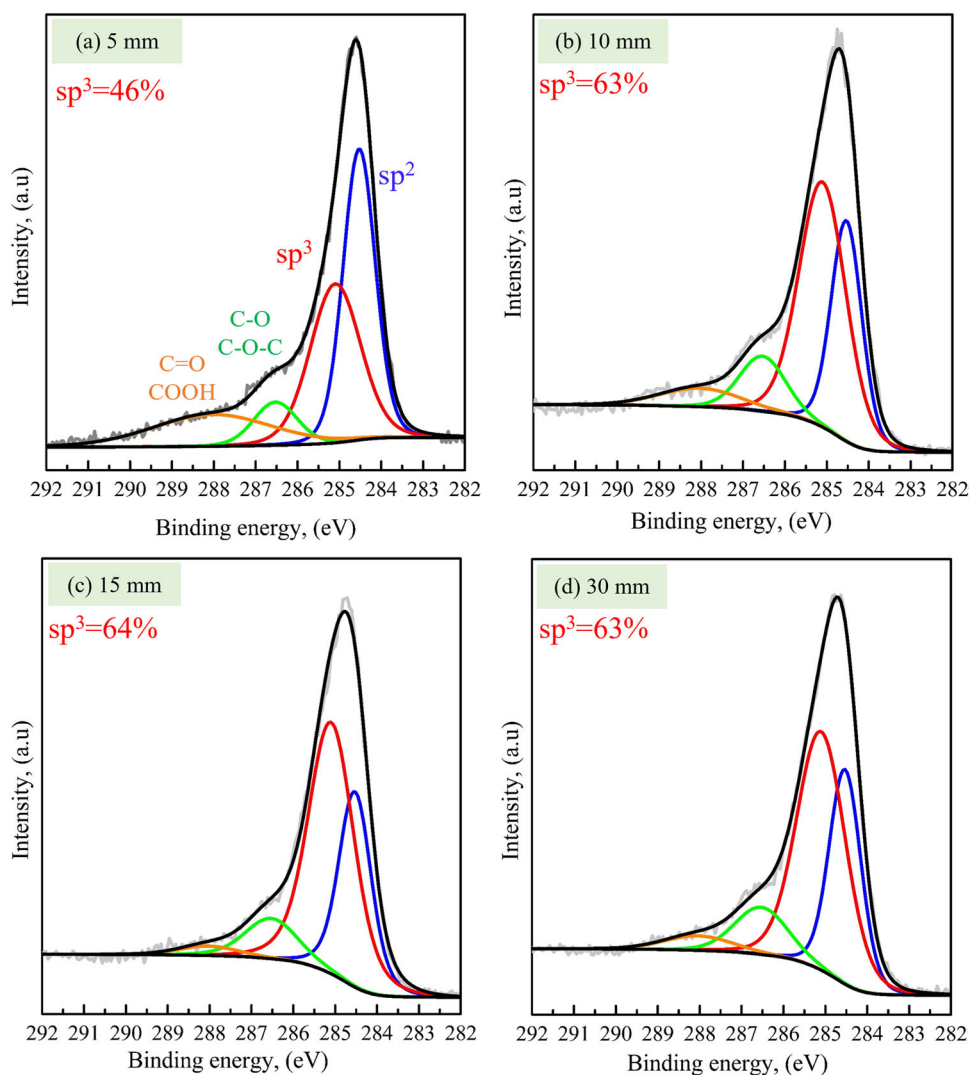
2.2 Films Characterization

2.2.1 Mechanical Properties

Mechanical properties, encompassing hardness and Young's modulus, were assessed utilizing a nanoindentation instrument (Picodentor HM500, Fischer Instrumentation, UK) featuring a Berkovich diamond indenter. The nanoindentation test applied a maximum load of 5 mN/10 s, and to ensure reliability, more than ten points on each sample, meticulously polished to a mirror-like finish, underwent indentation load–displacement measurements. Adhesion strength of the fabricated films underwent assessment via a blasting adhesion test (Anton Paar RST³). This involved using silicon carbide (SiC#800) particles subjected to dynamic blasting pressures of 0.35 MPa for 10-s exposure time. The evaluation criterion was the time required for film detachment in the blasting spot area. The critical blasting time was ascertained by inspecting damaged areas and removed volume using an optical microscope. Furthermore, adhesion between the WC–Co substrate and NDC coatings was evaluated through Rockwell D indentation tests, employing a load of 100 kg.



Fig. 4 C 1s X-ray photoelectron spectra of NDC films deposited at various TSDs: (a) 5, (b) 10, (c) 15, and (d) 30 mm



To understand the cause behind the film's adhesion, the internal stress in NDC film was assessed using curvature method. Thin NDC film with thickness in the range of 134–175 nm was deposited on unheated 260 μm Si (100) substrate with dimensions of 15 mm \times 5 mm at various TSD of 5, 10, and 15 mm. The bending deflection curve was measured parallel to the Si [111] direction of the long side (15 mm) using a surface roughness meter while the sample was fixed from only one side.

2.2.2 Structural Properties

Structural properties of the films were investigated to elucidate the correlation between mechanical properties and the C sp^3 ratio in the films concerning variations in TSDs, the film structure was investigated using X-ray photoelectron spectra (XPS) at beam line 12 (BL12) of SAGA Light Source/Kyushu Synchrotron Light Research Center. Initial

examination of the films' elemental composition was conducted through survey measurements across a binding energy range of 0–1000 eV, employing a monochromatic $\text{MgK}\alpha$ line ($h\nu = 1253.6$ eV). Subsequent detailed XPS measurements, utilizing synchrotron radiation with an incident photon energy of 350 eV, included background subtraction using the Shirley method before peak decomposition analyses. Critical parameters, such as film thickness, measured with a profilometer alongside deposition time, and film morphologies observed through top-view images obtained by field-emission scanning electron microscopy (FE-SEM) from JEOL (JSM-IT700HR), were integral to this investigation. Additionally, the surface roughness of the deposited NDC films was assessed using a 3D laser confocal microscope (LEXT OLS5000, Olympus, Japan), providing a comprehensive perspective on the films' structural properties including various factors of surface roughness.

3 Results and Discussion

3.1 Mechanical and Correlated Structural Characteristics of NDC Coatings

3.1.1 Nanoindentation Measurements

The mechanical properties of the deposited NDC films were systematically evaluated through nanoindentation tests, varying the TSDs in the range of 5–50 mm. Figure 2 depicts the films' measured hardness and Young's modulus as functions of TSDs. Notably, the film deposited at a TSD of 5 mm exhibited the lowest hardness at 31.6 GPa and the highest Young's modulus at 707 GPa. Films deposited with TSDs ranging from 10 to 50 mm displayed a hardness fluctuation between 48.4 and 51.3 GPa, while Young's modulus changed from 420 to 546 GPa. The film deposited at a TSD of 15 mm achieved the maximum hardness of 51.3 GPa with a Young's modulus of 520 GPa.

To comprehend the relationship between film hardness and TSD values, elemental composition analysis and determination of the C sp^3 fraction within the NDC films were conducted through decomposition of XPS spectra. Figure 3 illustrates the XPS survey of films deposited at various TSDs. In addition to the O KLL peak, attributed to the Auger effect, intense C 1s and O 1s peaks were observed. The O 1s peaks were ascribed to oxygen adsorption during or after film deposition [43, 44].

For a quantitative assessment of the $sp^3/(sp^2 + sp^3)$ ratio, denoted as the C sp^3 fraction, the C 1s spectra (Fig. 4) underwent deconvolution into four peaks. The sp^3 fraction was estimated from the areas of the decomposed sp^3 and sp^2 peaks, representing sp^2 -bonded carbon (C=C), sp^3 -bonded carbon (C–C), carbon–oxygen single bonds (C–O/C–O–C), and carbon–oxygen double bonds (C=O/COOH) [45]. These peaks were assigned at the binding energies of 284.5, 285.07, 286.57, and 288.32 eV, respectively. The resulting shoulder peaks of C–O/C–O–C and C=O/COOH may have originated from oxygen adsorption on the film surface during and after film deposition [44].

The resulting sp^3 fraction correlated well with the measured hardness and Young's modulus values as shown in Fig. 5. The film deposited at a TSD of 5 mm exhibited the lowest hardness and a-C sp^3 fraction of 46%, while the trend in hardness for the other films aligned with their respective sp^3 fractions. The film deposited at a TSD of 15 mm exhibited a sp^3 fraction of 64% while the films deposited at TSD of 10 mm exhibited C sp^3 fraction of 63%. The influence of C–C bonds on sharpening sp^3 peaks is well-known, underscoring the role of sp^2 and sp^3 bond fractions in determining the hardness of NDC films. To comprehensively unravel the correlation between mechanical and structural properties resulting from TSD variations, the subsequent sections

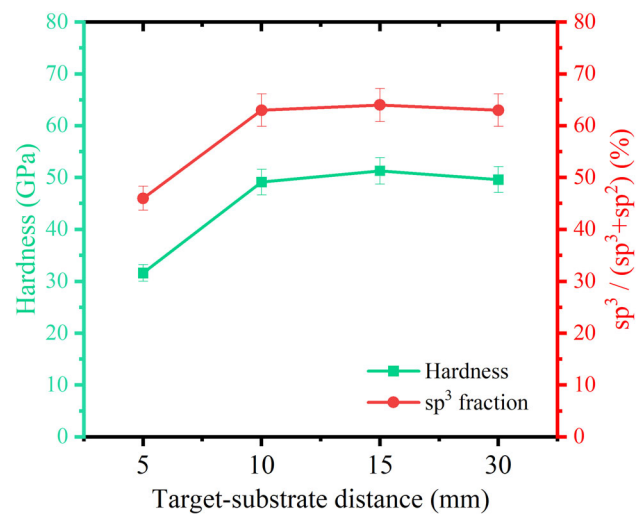


Fig. 5 Correlation between hardness and sp^3 fraction of deposited NDC films

will delve into the discussion of films' growth mechanisms and topography.

3.1.2 Adhesion Assessment of NDC Films

Evaluation of adhesion strength is paramount in assessing the performance of hard coatings, alongside hardness and Young's modulus. A blasting adhesion test, utilizing silicon carbide particles (SiC#800), was conducted to appraise the adhesion between NDC films and substrates as shown in Fig. 6a, b, and c. Remarkably, the film fabricated at a TSD of 10 mm exhibited exceptional adhesion, resisting the effects of blasting. Conversely, an evident reduction in adhesion resistance was observed with increasing TSD. The heightened arrival of high-energy atoms at shorter TSDs likely facilitated a more robust interaction at the NDC film-substrate interface. However, the coating deposited at 5 mm and room temperature did not display improved adhesion, potentially due to residual stresses induced by the influx of energetic atoms.

For a more comprehensive understanding of film adhesion and toughness at varying TSD values, Rockwell D tests were conducted with a maximum load of 100 kg. Optical images in Fig. 6d,e, and f illustrate the indentation craters on NDC coatings after Rockwell testing. Films deposited at TSDs larger than 5 mm exhibit minimal coating cracks and spallation, indicating enhanced adhesion. In contrast, films deposited at TSD-5 mm display pronounced spalling and delamination under the same conditions. Toughness measurements align with the blasting adhesion test results, highlighting that the optimal TSD for NDC fabrication is 10 mm.

To understand the physical origin of the change in adhesion properties, internal stress was assessed. Figure 7 depicts the bending deflection curve of an NDC film deposited on a



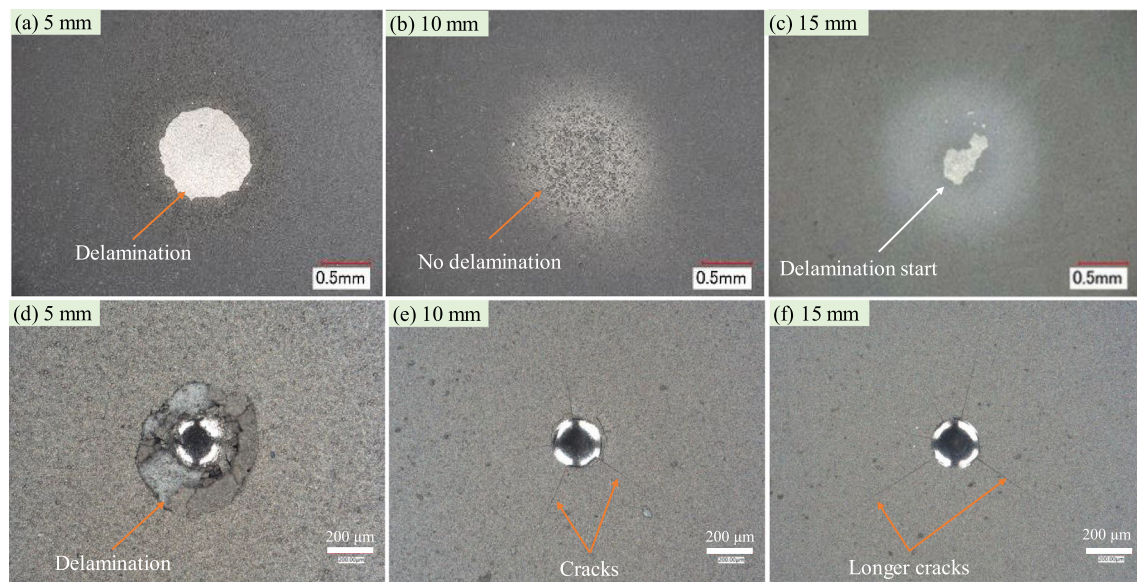


Fig. 6 Microscopic images resulting from a 10-s SiC#800 particle blasting test **a**, **b**, and **c** and Rockwell D test **d**, **f**, and **e** conducted on NDC films deposited at different TSDs

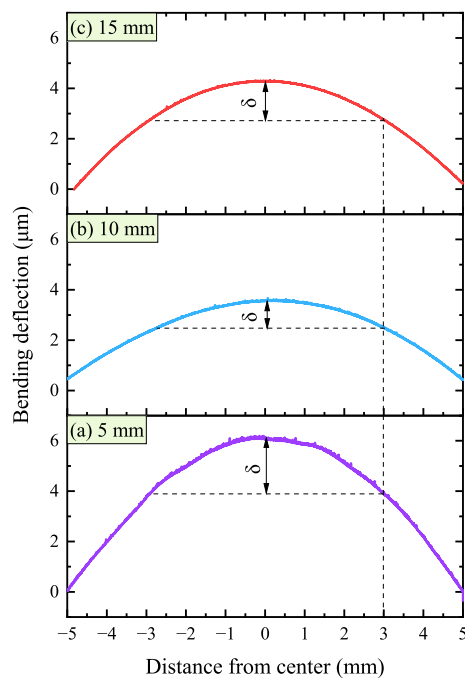


Fig. 7 Bending deflection curve of NDC films deposited at various TSD of **a** 5 mm, **b** 10 mm, and **c** 15 mm on 260-μm Si (100) substrate at room temperature, measured along Si [110] by surface roughness meter

Si (100) substrate, revealing the curvature as a reflection of internal stress. The measured profile exhibits a convex shape, indicative of compressive internal stress within the film. The obtained bending deflection (δ) aligns qualitatively with the adhesion resistance observed in both the blasting and Rockwell tests. Utilizing Stoney's formula presented in Eq. (1)

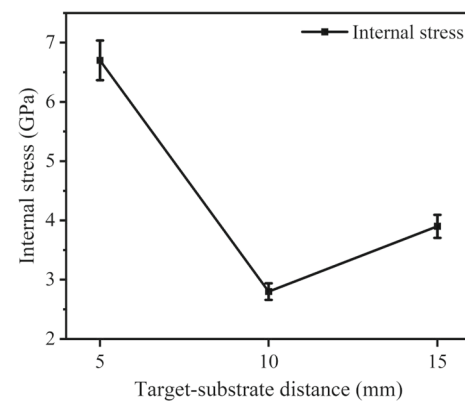


Fig. 8 Quantified internal stress in NDC films deposited at different TSDs: 5, 10, and 15 mm

for long and narrow samples, the internal stress (σ) was estimated at 6.7, 2.8, and 4.5 GPa for films deposited at TSDs of 5, 10, and 15 mm, as depicted in Fig. 8. This analysis underscores that the optimal TSD is 10 mm, where the film exhibits the lowest internal stress. In contrast, the film deposited at 5 mm TSD introduces the highest internal stress of 6.7 GPa, degrading to 4.5 GPa as TSD exceeds the optimal value and reaches 15 mm.

$$\sigma = \frac{E_s t_s^2 \delta}{3(1 - \nu_s) I^2 t_f} \quad (1)$$

Within this framework, E_s , t_s , and ν_s signify the Young's modulus, thickness, and Poisson's ratio of the Si substrate, respectively. Correspondingly, δ , I , and t_f denote the bending

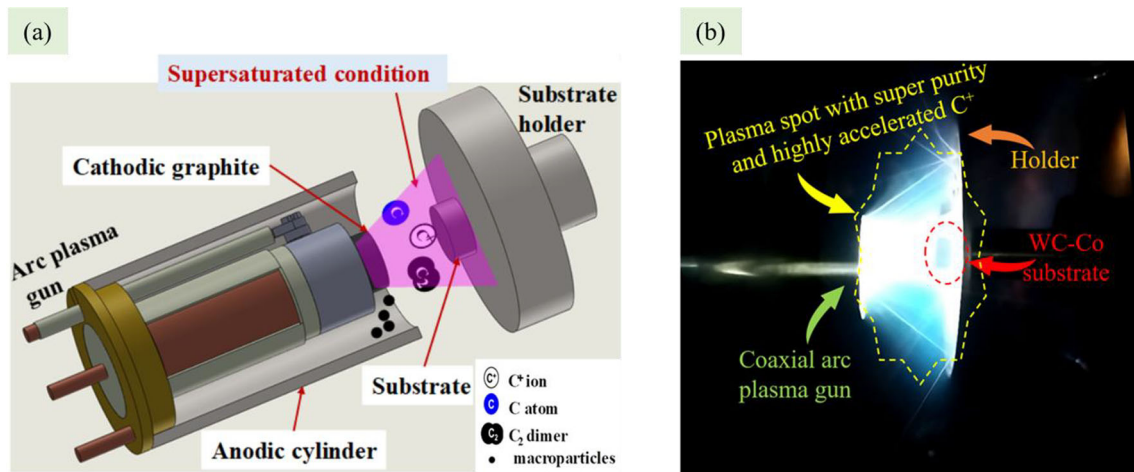


Fig. 9 Operational mechanism of CAPD apparatus: schematic diagram (Left) and real photo during deposition (Right)

deflection, distance from the center, and film thickness. The measurement of δ is based on the curvature of the film.

3.2 Growth Properties and Surface Topography of NDC Coatings

The investigation into the growth properties and surface topography of NDC coatings under various TSDs in the arc discharge plasma process revealed significant insights. Growth properties encompass film characteristics vital for formation and thickness during CAPD deposition, including deposition rate, film thickness, and the supersaturated state. Figure 9 illustrates a schematic diagram of the arc plasma gun and the resulted C species along with a typical photo image of the CAPD-plasma plume. The distribution of C species in plasma plume is illustrated at three TSDs, including optimal at 10 mm, reduced at 5 mm, and increased at 50 mm as shown in Fig. 10. Analysis of arc plasma emission indicated a notably high proportion of C^+ ions compared to C atoms and C_2 dimers [46, 47], with energetic C^+ ions playing a pivotal role in diamond growth. The variation in TSD resulted in different supersaturated conditions, influencing diamond growth and film characteristics. At the reduced TSD, the presence of macroparticles (Fig. 10-a) negatively impacted the supersaturated state, leading to increased sp^2 fraction and thus degraded mechanical properties with larger deposition rate leading to film thickness. At the optimal TSD (Fig. 10-b), a robust supersaturated state facilitates diamond grain growth, yielding improved mechanical properties. When the TSD increased, the number of C^+ ions reaching the substrate naturally decreased due to energy loss during travel (Fig. 10-c).

The deposition rate of NDC coatings exhibited a significant dependence on TSD (Fig. 11). Deposition at 5 mm TSD resulted in a rate of 2.19 nm/s, while at 50 mm TSD,

it dropped to 0.19 nm/s. This decline in deposition rate can be attributed to the reduced efficiency of the coating process with increasing TSD, causing deceleration of carbon species ejected from the graphite cathode. Furthermore, the resulted film thickness during a fixed deposition time of approximately 3 h shows sharp decreasing from 21.88 to 1.8 μm in the range of 5–50 mm as summarized in Fig. 12. Notably, films deposited at a 10 mm TSD exhibited hardness of 49.12 GPa and demonstrated a compelling deposition rate of 1.05 nm/s, three times higher than the film deposited at a TSD of 15 mm, which exhibited the maximum hardness of 51.3 GPa. This suggests that the film deposited at a TSD of 10 mm presents the most cost-effective option.

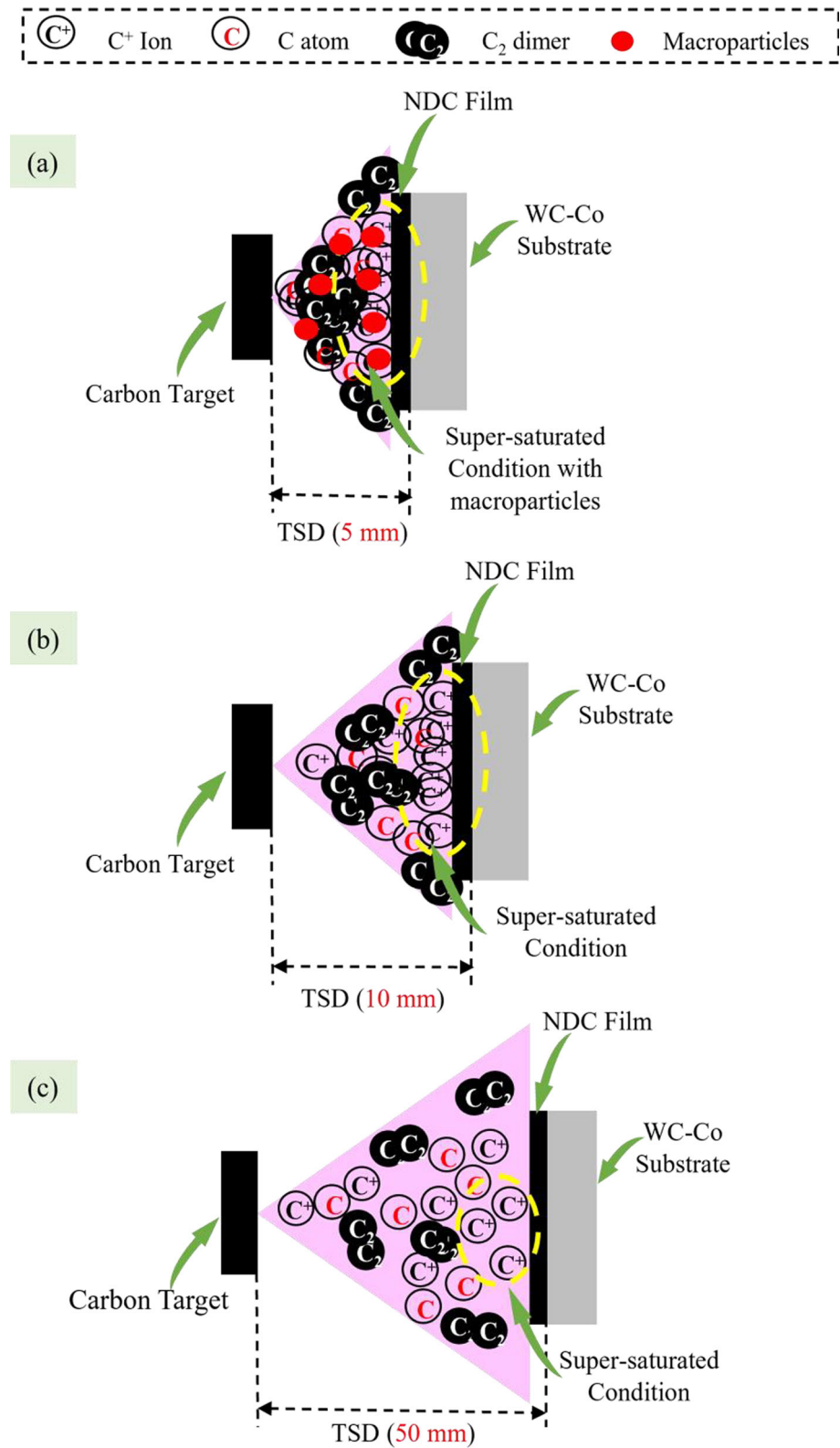
The NDC films exhibit superior hardness and Young's modulus when compared to conventional hard DLC films, showcasing performance comparable to ta-C coatings, as illustrated in Fig. 13. Notably, unlike ta-C films with thickness limitations in the range of a few hundred nanometers, NDC hard coatings can be successfully fabricated to thicknesses exceeding several micrometers ($\geq 11 \mu\text{m}$), akin to diamond coatings. This distinctive characteristic distinguishes NDC films from traditional DLC films and positions them as highly appealing for diverse applications.

The novel CAPD method employed allowed NDC film deposition without the need for external substrate heating or Co etching from the substrate surface. The film surface displayed a distinctive composition of particles with boundaries, exhibiting a cauliflower-type topography due to insufficient incident ion energy to overcome surface diffusion barriers. Surface morphologies of the NDC films (Fig. 14) showed homogeneous coated substrates' surfaces. The clusters becoming smaller and denser as TSD increased.

The topographical features and surface roughness of NDC films, synthesized under various TSD values, were evaluated using a 3D laser confocal microscope, as illustrated in



Fig. 10 Illustrations depicting the growth process of NDC films at TSD of **a** 5 mm, **b** 10 mm, and **c** 50 mm



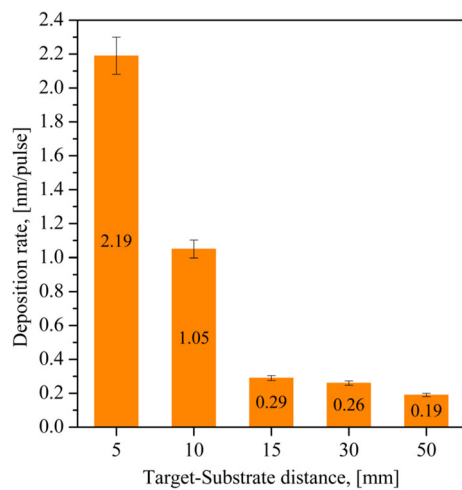


Fig. 11 Deposition rate of NDC films at different TSDs

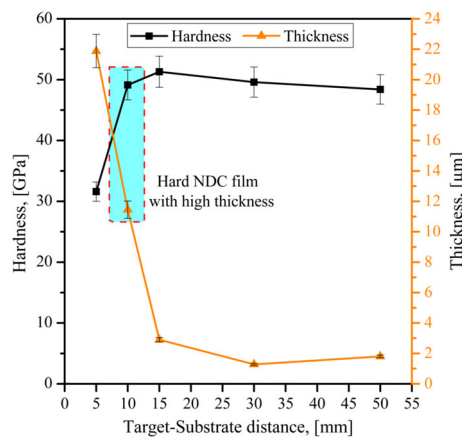


Fig. 12 Optimal thick and hard NDC films produced under varying TSDs during a constant deposition time of 10,000 s (~ 3 h)

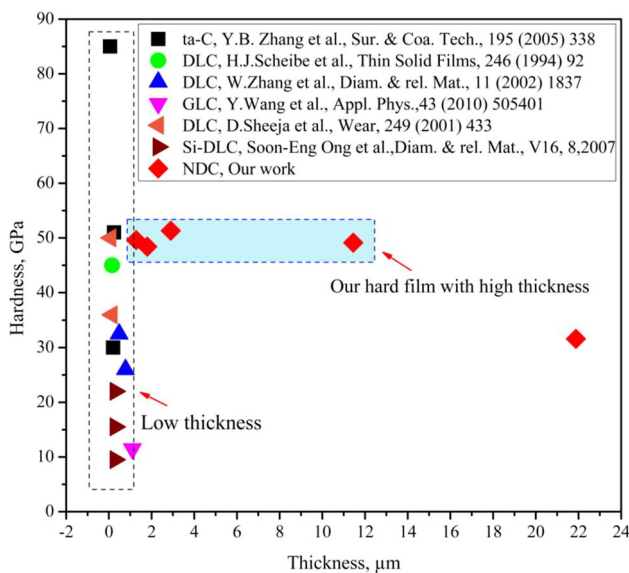


Fig. 13 Comparative analysis of hardness and thickness between NDC films and hard a-C films

Fig. 15. An evident reduction in surface roughness parameters, including Ra, Rz, Sa, and Sz, was observed with increasing TSD from 5 to 30 mm, signifying the efficient elimination of droplets and the high purity of the CAPD plasma. The Sa values decreased from 580 nm for the 5 mm TSD film to 280 nm for the 10 mm TSD film, followed by a further reduction to 179 nm for the film deposited at 15 mm TSD. This suggests that TSD values of 10 and 15 mm can yield films with comparable hardness around 50 GPa. However, films deposited at 10 mm TSD exhibit superior adhesion and thickness compared to those deposited at 15 mm TSD. Surprisingly, for applications emphasizing lower surface roughness with reasonable film thickness (3 μm), a TSD of 15 mm is recommended.

4 Conclusion

This study systematically investigated the impact of TSD variations (ranging from 5 to 50 mm) on NDC films deposited on unheated WC–Co substrates using the innovative CAPD method. Optimal film attributes were discerned at 10 mm TSD, characterized by a remarkable hardness of 49.12 GPa, a Young's modulus of 546 GPa, and a threefold higher deposition rate compared to the 15 mm TSD film. Structural analysis using XPS revealed variations in the C sp^3 fraction, influencing mechanical properties. A correlation between film hardness and TSD was established through XPS analysis, with the film at 5 mm TSD exhibiting the lowest C sp^3 fraction (46%) and corresponding lower hardness (31.6 GPa). Adhesion assessments highlighted superior adhesion resistance at 10 mm TSD, supported by Rockwell D indentation tests, and the physical origin was unveiled through internal stress estimation. Growth properties and surface topography studies disclosed TSD impacts on film thickness and surface characteristics. Particularly, films at 10 mm TSD demonstrated an intriguing deposition rate of 1.05 nm/s, rendering them a cost-effective choice. Furthermore, these films outperformed traditional DLC films in hardness and Young's modulus, positioning them as a promising alternative for diverse applications. This comprehensive exploration provides valuable insights into tailoring NDC film properties by adjusting TSD values, emphasizing the potential for producing high-performance, adherent thick films with controlled characteristics for various technological applications. Future research endeavors should prioritize investigating tribological properties while optimizing deposition parameters such as target energy and applied biased voltage on the substrate to enhance film properties for practical applications.



Fig. 14 Top-view SEM images of different NDC films deposited at TSDs of (a) 5, (b) 10, (c) 15, and (d) 30 mm

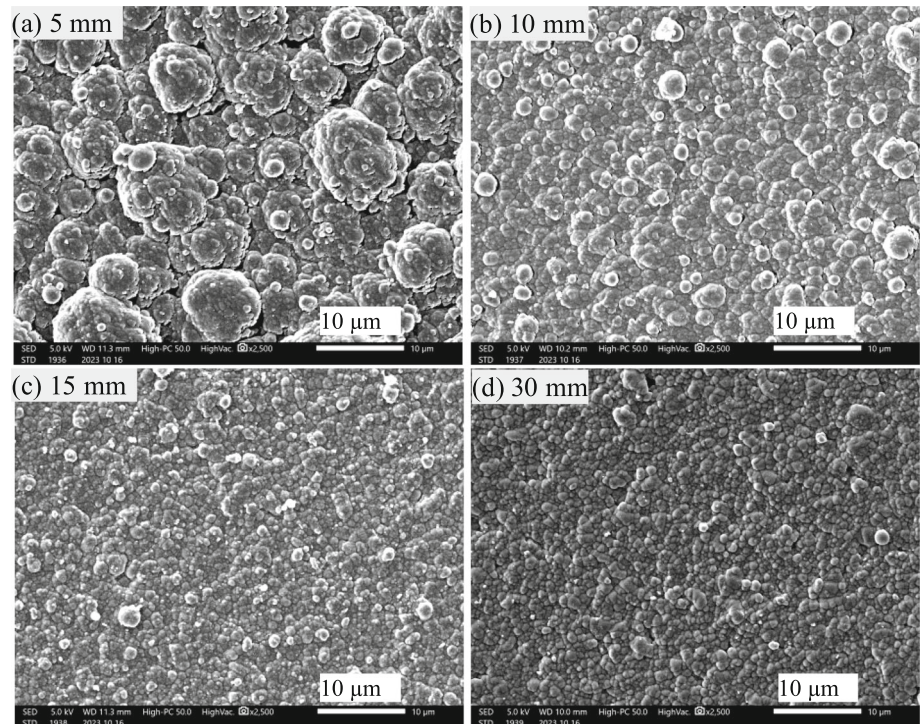
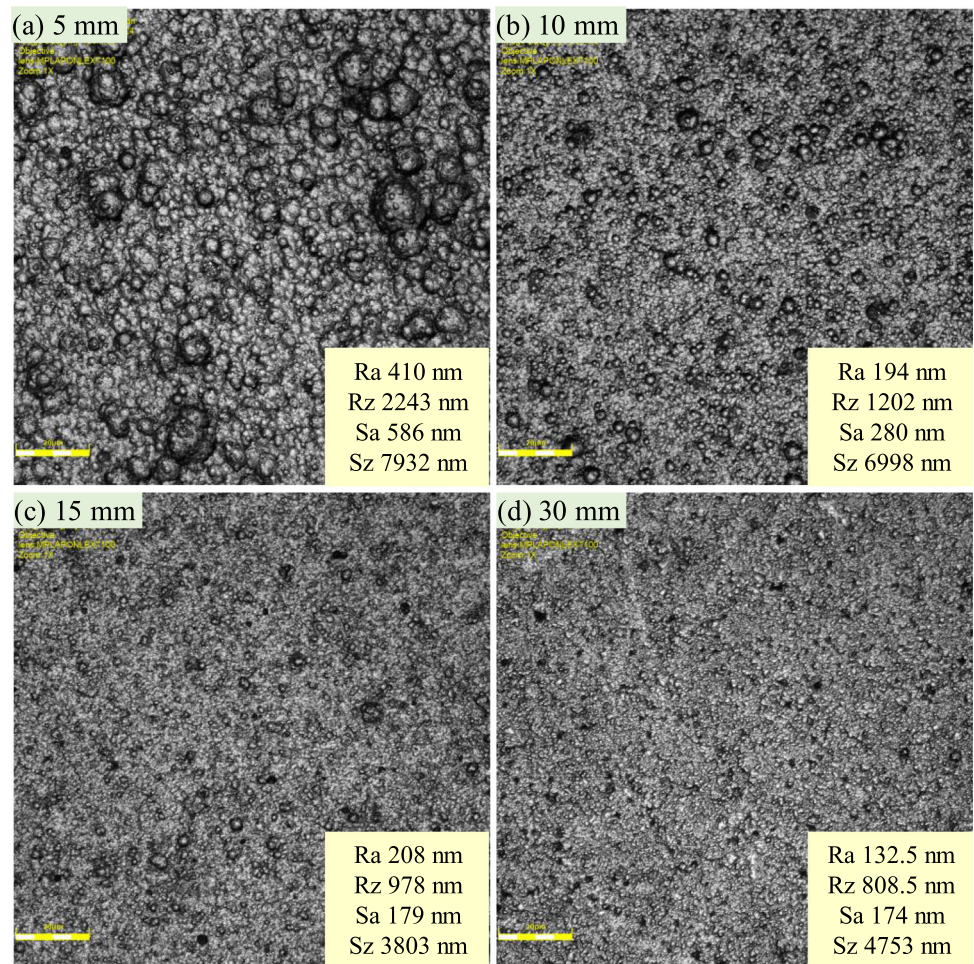


Fig. 15 Variations in surface morphologies of NDC films examined using 3D laser confocal microscopy across different TSDs: (a) 5, (b) 10, (c) 15, and (d) 30 mm



Acknowledgements The corresponding author (Mohamed Egiza) expresses gratitude to the Cultural Affairs and Missions Sector, Ministry of Higher Education, for their financial support. Additionally, this study received financial backing from the Osawa Scientific Studies Grants Foundation, Advanced Machining Technology & Development Association, JST A-STEP Stage II (seed development type AS2915051S), and JSPS KAKENHI Grant Nos. JP19H02436 and 21K18830. The XPS measurements were conducted at BL 12 of Kyushu Synchrotron Light Research Center/Saga Light Source under Proposal Nos. 1704022S, 2009085S, and 2106055S.

Author Contributions Mohamed Egiza was involved in conceptualization, project administration, writing—original draft preparation, formal analysis, methodology, and writing—reviewing and editing. Mohamed R. Diab (Ph.D student) contributed to validation, visualization, and methodology. Koki Murasawa and Hiroshi Naragino were responsible for visualization and methodology. Tsuyoshi Yoshitake took part in supervision, funding acquisition, and writing—reviewing and editing.

Data Availability Up on request.

Code Availability Not applicable.

Declarations

Conflict of interest The authors declare there is no conflict of interest financially or non-financially, directly or indirectly related to the work.

Ethical Approval Not applicable.

Open Access This article is licensed under a Creative Commons Attribution 4.0 International License, which permits use, sharing, adaptation, distribution and reproduction in any medium or format, as long as you give appropriate credit to the original author(s) and the source, provide a link to the Creative Commons licence, and indicate if changes were made. The images or other third party material in this article are included in the article's Creative Commons licence, unless indicated otherwise in a credit line to the material. If material is not included in the article's Creative Commons licence and your intended use is not permitted by statutory regulation or exceeds the permitted use, you will need to obtain permission directly from the copyright holder. To view a copy of this licence, visit <http://creativecommons.org/licenses/by/4.0/>.

References

- Wang, X.; Shen, X.; Zeng, C.; Sun, F.: Combined influences of tool shape and as-deposited diamond film on cutting performance of drills for CFRP machining. *Surf. Coat. Technol.* **347**, 390–397 (2018)
- Eckart Uhlmann, D.H.; Reimers, W.; Botther, K.: Multilayer structure dependent performance behaviour of CVD diamond thin film drilling tools during CFRP machining. *Procedia CIRP* **87**, 360 (2020)
- Zhang, J.; Wang, X.; Shen, B.; Sun, F.: Effect of boron and silicon doping on improving the cutting performance of CVD diamond coated cutting tools in machining CFRP. *Int. J. Refract Metal Hard Mater.* **41**, 285–292 (2013)
- Chakravarthy, G.V.; Chandran, M.; Bhattacharya, S.S.; Rao, M.R.; Kamaraj, M.: A comparative study on wear behavior of TiN and diamond coated WC–Co substrates against hypereutectic Al–Si alloys. *Appl. Surf. Sci.* **261**, 520–527 (2012)
- Bouzakis, K.-D.; Michailidis, N.; Skordaris, G.; Bouzakis, E.; Biermann, D.; M'Saoubi, R.: Cutting with coated tools: coating technologies, characterization methods and performance optimization. *CIRP Ann.* **61**(2), 703–723 (2012)
- Campos, R.A.; Contin, A.; Trava-Airoldi, V.J.; Barquete, D.M.; Corat, E.J.: CVD of alternated MCD and NCD films on cemented carbide inserts. *J. ASTM Int.* **8**(3), 1–10 (2011)
- Polini, R.; Barletta, M.: On the use of CrN/Cr and CrN interlayers in hot filament chemical vapour deposition (HF-CVD) of diamond films onto WC–Co substrates. *Diam. Relat. Mater.* **17**(3), 325–335 (2008)
- Choy, K.-L.: Chemical vapour deposition (CVD): advances, technology and applications. CRC Press, Boca Raton (2019)
- Sein, H.; Ahmed, W.; Jackson, M.; Polini, R.; Hassan, I.; Amar, M.; Rego, C.: Enhancing nucleation density and adhesion of polycrystalline diamond films deposited by HFCVD using surface treatments on Co cemented tungsten carbide. *Diam. Relat. Mater.* **13**(4), 610–615 (2004)
- Gupta, G.; Tyagi, R.; Rajput, S.; Saxena, P.; Vashisth, A.; Mehndiratta, S.: PVD based thin film deposition methods and characterization/property of different compositional coatings—a critical analysis. *Mater. Today Proc.* **38**, 259–264 (2021)
- Straffellini, G.; Scardi, P.; Molinari, A.; Polini, R.: Characterization and sliding behavior of HFCVD diamond coatings on WC–Co. *Wear* **249**(5), 461–472 (2001)
- Arya, A.K.; Parmar, R.; Gour, K.; Gunnella, R.; Rosolen, J.; Singh, V.: Chemical vapor deposition (CVD) technique for nanomaterials deposition. In: *Chemical methods for processing nanomaterials*, pp. 125–146. CRC Press, Boca Raton (2021)
- Windischmann, H.; Epps, G.F.; Cong, Y.; Collins, R.: Intrinsic stress in diamond films prepared by microwave plasma CVD. *J. Appl. Phys.* **69**(4), 2231–2237 (1991)
- Rajak, D.K.; Kumar, A.; Behera, A.; Menezes, P.L.: Diamond-like carbon (DLC) coatings: classification, properties, and applications. *Appl. Sci.* **11**(10), 4445 (2021)
- Vetter, J.: 60years of DLC coatings: Historical highlights and technical review of cathodic arc processes to synthesize various DLC types, and their evolution for industrial applications. *Surf. Coat. Technol.* **257**, 213–240 (2014)
- Zhang, D.; Shen, B.; Sun, F.: Study on tribological behavior and cutting performance of CVD diamond and DLC films on Co-cemented tungsten carbide substrates. *Appl. Surf. Sci.* **256**(8), 2479–2489 (2010)
- Robertson, J.: Diamond-like amorphous carbon. *Mater. Sci. Eng. R. Rep.* **37**(4), 129–281 (2002)
- Grill, A.: Tribology of diamondlike carbon and related materials: an updated review. *Surf. Coat. Technol.* **94–95**, 507–513 (1997)
- Baptista, A.; Silva, F.; Porteiro, J.; Míguez, J.; Pinto, G.: Sputtering physical vapour deposition (PVD) coatings: a critical review on process improvement and market trend demands. *Coatings* **8**(11), 402 (2018)
- Mochalin, V.N.; Shenderova, O.; Ho, D.; Gogotsi, Y.: The properties and applications of nanodiamonds. *Nat. Nanotechnol.* **7**(1), 11–23 (2012)
- Ali, A.M.; Egiza, M.; Murasawa, K.; Sugita, H.; Deckert-Gaudig, T.; Deckert, V.; Yoshitake, T.: Effects of substrate temperature and intermediate layer on adhesion, structural and mechanical properties of coaxial arc plasma deposition grown nanodiamond composite films on Si substrates. *Surf. Coat. Technol.* **417**, 127185 (2021)
- Egiza, M.; Murasawa, K.; Ali, A.M.; Fukui, Y.; Gonda, H.; Sakurai, M.; Yoshitake, T.: Enhanced hardness of nanocarbon films deposited on cemented tungsten carbide substrates by coaxial plasma deposition owing to employing silicon-doped graphite targets. *Jpn. J. Appl. Phys.* **58**(7), 075507 (2019)



23. Naragino, H.; Egiza, M.; Tominaga, A.; Murasawa, K.; Gonda, H.; Sakurai, M.; Yoshitake, T.: Hard coating of ultrananocrystalline diamond/nonhydrogenated amorphous carbon composite films on cemented tungsten carbide by coaxial arc plasma deposition. *Appl. Phys. A* **122**, 1–10 (2016)
24. Egiza, M.; Naragino, H.; Tominaga, A.; Murasawa, K.; Gonda, H.; Sakurai, M.; Yoshitake, T.: Si and Cr doping effects on growth and mechanical properties of ultrananocrystalline diamond/amorphous carbon composite films deposited on cemented carbide substrates by coaxial arc plasma deposition. *EVERGR. Jt. J. Novel Carbon Resour. Sci. Green Asia Strateg.* **03**(01), 5 (2016)
25. Egiza, M.; Naragino, H.; Tominaga, A.; Hanada, K.; Kamitani, K.; Sugiyama, T.; Ikenaga, E.; Murasawa, K.; Gonda, H.; Sakurai, M.: Effects of air exposure on hard and soft X-ray photoemission spectra of ultrananocrystalline diamond/amorphous carbon composite films. *Coatings* **8**(10), 359 (2018)
26. Egiza, M.; Ragab Diab, M.; Ali, A.M.; Murasawa, K.; Yoshitake, T.: Sustainable super-hard and thick nanodiamond composite film deposited on cemented carbide substrates with an interfacial Al-interlayer. *Mater. Lett.* **364**, 136369 (2024)
27. Ali, A.M.; Deckert-Gaudig, T.; Egiza, M.; Deckert, V.; Yoshitake, T.: Near- and far-field Raman spectroscopic studies of nanodiamond composite films deposited by coaxial arc plasma. *Appl. Phys. Lett.* **116**(4), 5 (2020)
28. Hanada, K.; Yoshida, T.; Nakagawa, Y.; Yoshitake, T.: Formation of ultrananocrystalline diamond/amorphous carbon composite films in vacuum using coaxial arc plasma gun. *Jpn. J. Appl. Phys.* **49**(12R), 125503 (2010)
29. Yoshitake, T.; Nagano, A.; Ohmagari, S.; Itakura, M.; Kuwano, N.; Ohtani, R.; Setoyama, H.; Kobayashi, E.; Nagayama, K.: Near-edge x-ray absorption fine-structure, x-ray photoemission, and Fourier transform infrared spectroscopies of ultrananocrystalline diamond/hydrogenated amorphous carbon composite films. *Jpn. J. Appl. Phys.* **48**(2R), 020222 (2009)
30. Naragino, H.; Egiza, M.; Tominaga, A.; Murasawa, K.; Gonda, H.; Sakurai, M.; Yoshitake, T.: Fabrication of ultrananocrystalline diamond/nonhydrogenated amorphous carbon composite films for hard coating by coaxial arc plasma deposition. *EVERGR. Jt. J. Novel Carbon Resour. Sci. Green Asia Strateg.* **03**(01), 5 (2016)
31. Ali, A.M.; Egiza, M.; Murasawa, K.; Fukui, Y.; Gonda, H.; Sakurai, M.; Yoshitake, T.: Negative bias effects on deposition and mechanical properties of ultrananocrystalline diamond/amorphous carbon composite films deposited on cemented carbide substrates by coaxial arc plasma. *Diam. Relat. Mater.* **96**, 67–73 (2019)
32. Egiza, M.; Ali, A.M.; Diab, M.R.; Hemaya, N.; Murasawa, K.; Yoshitake, T.: Synthesis and comprehensive synchrotron-based structural analysis of Si-doped nanodiamond composite films deposited on cemented carbide. *Surf. Coat. Technol.* **471**, 129867 (2023)
33. Egiza, M.; Naragino, H.; Tominaga, A.; Murasawa, K.; Gonda, H.; Sakurai, M.; Yoshitake, T.: B-doped nanodiamond composite hard coatings deposited on cemented carbide: Mechanical, structural, and tribological properties. *Int. J. Refract. Metals Hard Mater.* **114**, 106260 (2023)
34. Diab, M.R.; Egiza, M.; Murasawa, K.; Ohmagari, S.; Naragino, H.; Yoshitake, T.: Revealing mechanical and structural properties of Si-doped nanodiamond composite films through applied biasing voltages on WC–Co substrates. *Int. J. Refract. Metals Hard Mater.* **119**, 106518 (2024)
35. Ali, A.M.; Egiza, M.; Murasawa, K.; Sugita, H.; Deckert-Gaudig, T.; Deckert, V.; Yoshitake, T.: Influence of adhesion intermediate layers on the stability of nanodiamond composite films deposited on Si substrates by coaxial arc plasma. *Appl. Phys. Express* **13**(6), 065506 (2020)
36. Osman, L.; Ali, A.M.; Zkria, A.; Naragino, H.; Yoshitake, T.: Adhesion of nanodiamond composite films on Ti substrates at room temperature via hybrid ion etching gun and coaxial arc plasma deposition. *Appl. Phys. Express* **15**(11), 115004 (2022)
37. Naragino, H.; Egiza, M.; Tominaga, A.; Murasawa, K.; Gonda, H.; Sakurai, M.; Yoshitake, T.: Fabrication of ultrananocrystalline diamond/nonhydrogenated amorphous carbon composite films for hard coating by coaxial arc plasma deposition. *Electr. Eng. Sci.* **3**(01), 1–5 (2016)
38. Diab, M.R.; Egiza, M.; Murasawa, K.; Naragino, H.; El-Shaer, A.; Yoshitake, T.: Eco-friendly thick and wear-resistant nanodiamond composite hard coatings deposited on WC–Co substrates. *Surf. Coat. Technol.* **479**, 130517 (2024)
39. Wuhner, R.; Yeung, W.Y.: Effect of target–substrate working distance on magnetron sputter deposition of nanostructured titanium aluminium nitride coatings. *Scr. Mater.* **49**(3), 199–205 (2003)
40. Hua, Q.; Ligang, W.; Ruijin, L.; Wenfeng, Y.: Influence of target substrate distance on the properties of transparent conductive Si doped ZnO thin films. *Optik* **125**(15), 3902–3907 (2014)
41. Dai, H.Y.; Du, J.; Zhan, C.: Role of target-substrate distance on the structural, mechanical and electrical properties of amorphous carbon films. *J. Mater. Sci. Mater. Electron.* **26**(9), 6552–6556 (2015)
42. Naragino, H.; Egiza, M.; Tominaga, A.; Murasawa, K.; Gonda, H.; Sakurai, M.; Yoshitake, T.: Room-temperature hard coating of ultrananocrystalline diamond/nonhydrogenated amorphous carbon composite films on tungsten carbide by coaxial arc plasma deposition. *Jpn. J. Appl. Phys.* **55**(3), 030302 (2016)
43. Ohmagari, S.; Yoshitake, T.; Nagano, A.; Ohtani, R.; Setoyama, H.; Kobayashi, E.; Nagayama, K.: X-ray photoemission spectroscopic study of ultrananocrystalline diamond/hydrogenated amorphous carbon composite films prepared by pulsed laser deposition. *Diam. Relat. Mater.* **19**(7–9), 911–913 (2010)
44. Egiza, M.; Naragino, H.; Tominaga, A.; Hanada, K.; Kamitani, K.; Sugiyama, T.; Ikenaga, E.; Murasawa, K.; Gonda, H.; Sakurai, M.; Yoshitake, T.: Effects of air exposure on hard and soft X-ray photoemission spectra of ultrananocrystalline diamond/amorphous carbon composite films. *Coatings* **8**(10), 359 (2018)
45. Zkria, A.; Abubakr, E.; Egiza, M.; Haque, A.; Narayan, J.; Yoshitake, T.: Structural evolution of laser-irradiated ultrananocrystalline diamond/amorphous carbon composite films prepared by coaxial arc plasma. *Appl. Phys. Express* **13**(10), 105503 (2020)
46. Naragino, H.; Tominaga, A.; Hanada, K.; Yoshitake, T.: Synthesis method for ultrananocrystalline diamond in powder employing a coaxial arc plasma gun. *Appl. Phys. Express* **8**(7), 075101 (2015)
47. Hanada, K.; Nishiyama, T.; Yoshitake, T.; Nagayama, K.: Time-Resolved Observation of Deposition Process of Ultrananocrystalline Diamond/Hydrogenated Amorphous Carbon Composite Films in Pulsed Laser Deposition. *J. Nanomater.* (2009). <https://doi.org/10.1155/2009/901241>

